Supporting Information

An All-in-one Free-Standing Single-Ion Conducting Semi-Solid Polymer Electrolyte for High-Performance Practical Li Metal Batteries

Jinping Zhang, [ac] Jie Zhu, [ac] Ruiqi Zhao, [ac] Jie Liu, [ac] Xingchen Song, [ac] Nuo Xu, [ac] Yansong Liu, [ac] Hongtao Zhang, *[ac] Xiangjian Wan, [abc] Yanfeng Ma, [ac] Chenxi Li, [ac] and Yongsheng Chen*[abc]

[a] *The Centre of Nanoscale Science and Technology and Key Laboratory of Functional Polymer Materials, Institute of Polymer Chemistry, College of Chemistry, Nankai University, Tianjin 300071, China*

[b] *State Key Laboratory of Elemento-Organic Chemistry, Nankai University, Tianjin, 300071, China*

[c] *Renewable Energy Conversion and Storage Center (RECAST), Nankai University, Tianjin 300071, China*

*Corresponding author.

E-mail address: yschen99@nankai.edu.cn; htzhang@nankai.edu.cn

Experimental Section

Materials:

Allylboronic acid pinacol ester (AAPE) and 2-hydroxy-2-methylpropiophenone (HMPP) were purchased from Aladdin. Pentaerythritol tetraacrylate (PETA) was purchased from Macklin. Poly (vinylidene fluoride-*co*-hexafluoropropylene) (PVDF-HFP) was purchased from Sigma-Aldrich. Lithium difluorophosphate (LiDFP), fluoroethylene carbonate (FEC), tetraethylene glycol dimethyl ether (G_4), dimethyl carbonate (DMC), and lithium bis(trifluoromethanesulfonyl)imide (LiTFSI) were purchased from Duoduo chemical company in Suzhou.

Electrolyte Preparation:

The PBSIL solid polymer electrolyte membranes were prepared by ultraviolet (UV) curing the precursor solution. Firstly, solvate ionic liquid (SIL) was prepared by mixing LiTFSI with G_4 in a molar ratio of 1 : 1 and stirring for 24 h at room temperature, in which LiDFP and FEC were added as additives with a content of 0.5 wt%, respectively. Subsequently, PVDF-HFP, SIL, AAPE, PETA, and HMPP with different mass ratios were dissolved in 10 mL anhydrous acetone at room temperature to get the precursor solution. The content of HMPP was kept at 3 wt%, respect to the total mass of AAPE and PETA. Then the precursor solution was drop-casted onto a flat glass dish and cured under UV light (365 nm) for 10 minutes. After vacuum drying at room temperature for 12 hours to remove residual acetone solvent, PBSIL electrolyte membranes were obtained. The PSIL electrolyte was prepared in the same way without the addition of AAPE. All processes of electrolyte preparation were conducted in an Ar-filled glove box (Mikrouna, $[O_2] < 0.01$ ppm, $[H_2O] < 0.01$ ppm).

Electrode Preparation and Battery Assembly:

$LiFePO_4$ (LFP), $LiNi_{0.8}Mn_{0.1}Co_{0.1}O_2$ (NCM811), $LiNi_{0.6}Mn_{0.2}Co_{0.2}O_2$ (NCM622), and $Li_{1.2}Mn_{0.54}Co_{0.13}Ni_{0.13}O_2$ (LMCNO) cathodes were prepared by casting uniformly dispersed slurry of active materials, super P, and poly(vinylidene fluoride) (PVDF) (8:1:1) onto Al foil and dried at 120 °C for 24 hours under vacuum. The cathode sheets were punched into round discs with a diameter of 10 mm. The cathodes had an active material mass loading of about 1.5 mg cm^{-2}. High-loading NCM811 cathodes for coin

and pouch cells were prepared by casting uniformly dispersed slurry of active materials, super P, LiTFSI, and poly(vinylidene fluoride) (PVDF) (7:1:1:1) onto carbon-coated Al foil and dried at 120 °C for 24 hours under vacuum. The cathodes had an active material mass loading of about 8.0 mg cm^{-2}. High-loading NCM811 cathode for cylindrical cell (approximately 8 mg cm^{-2}) cathode was purchased from Guangdong Canrd New Energy Technology Co., Ltd. Ultra-thin Li foil (20 μm) was purchased from China Energy Lithium Co., Ltd. CR2025 type coin cell or pouch cell was assembled by sandwiching PBSIL electrolyte membrane between the cathode and Li anode. Cylindrical cell was assembled by placing the high-loading NCM811 cathode, ultra-thin Li anode and PBSIL electrolyte with the corresponding size on the winding machine for winding into a jelly roll, and then the jelly roll was inserted into the 18650 cell can for sealing. Z-stacked pouch cell was assembled by stacking two high-loading cathode pieces, three PBSIL electrolyte pieces, and two ultra-thin Li anode pieces on top of each other in line with the Z-shaped pouch cell. All processes of cell assembly were conducted in an Ar-filled glove box (Mikrouna, $[O_2] < 0.01$ ppm, $[H_2O] < 0.01$ ppm).

Material Characterization:

Fourier transform infrared spectroscopy (FT-IR) measurements were carried on Thermo Scientific Nicolet iS50 FT-IR spectrometer in the wavelength range of 400-4000 cm^{-1} through the attenuated total reflection (ATR) model. The stress-strain test of the sample was performed on a UTM6103 mechanical testing instrument (Shenzhen Suns Technology Stock Co., LTD., China) with a tensile speed of 5 mm min^{-1}. The thermogravimetric analysis (TGA) was carried out on a NETZSCH STA 409PC instrument under purified nitrogen gas flow with a heating rate of 10 K min^{-1}. The cycled electrode sample (Li anode or NCM811 cathode) was obtained by disassembling the battery, stripping PBSIL from the surface, and washing the electrode with DMC more than five times to remove residual electrolytes before characterization. The morphology of the electrode was observed by the Phenom SEM system. X-ray photoelectron spectroscopy (XPS) was taken on an ESCALAB 250 Xi (Thermo Fisher Scientific Inc., USA) with monochromatic 150 W Al Kα radiation. Solid-state nuclear

magnetic resonance spectroscopy (ssNMR) experiment was performed on a Bruker AVANCE NEO wide-bore (89 mm) NMR spectrometer at a ^{7}Li frequency of 155.66 MHz. A 2.5mm probe was used, the MAS frequency was automatically controlled at 15 kHz. The ^{7}Li chemical shifts were referenced to LiCl solution (1.1 ppm).

Electrochemical measurement:

Electrochemical impedance spectroscopy (EIS), linear sweep voltammetry (LSV), and chronoamperometry tests were conducted by using a Vionic (Metrohm). The electrochemical floating analysis and the electrochemical cycle tests of Li||Li, Li||LFP, Li||NCM811, Li||NCM622 and Li||LMCNO were performed using a LAND battery testing system (Land CT2001A model, Wuhan LAND Electronics. Ltd.). The ionic conductivities of the PBSIL electrolytes were tested by electrochemical impedance spectroscopy with an amplitude of 5 mV over the frequency range of $0.1-10^{6}$ Hz at the open-circuit potential (OCP) and a temperature range from 25 to 60 °C in the stainless steel (SS)||SS cell. The ionic conductivity was calculated according to the following equation

$$\sigma = L / RS$$

where R, L, and S are the bulk resistance, thickness, and area of the electrolyte sample, respectively. The activation energy of Li^{+} transport was calculated based on the following equation

$$\sigma = A \exp (-E_a / RT)$$

where A is the pre-exponential factor, E_a is the activation energy of Li^{+} transport, R is the ideal gas constant, and T is the testing absolute temperature. The LSV test was recorded from 3 to 6 V versus Li^{+}/Li at a scanning rate of 1 mV s^{-1}, and the measured electrolyte was assembled in Li||SS cell. The chronoamperometry test of Li||Al coin cell for 5 h at 5.0 V was performed after a LSV scan from the OCP to 5.0 V at a scan rate of 1.0 mV s^{-1}. The Li^{+} transference number (t_{Li+}) was estimated by the electrochemical polarization method in Li||Li symmetric cell and was calculated by the following equation

$$t_{Li+} = I_s(\Delta V - I_0R_0) / I_0(\Delta V - I_sR_s)$$

where I_0 and I_s are the initial and steady currents during polarization, R_0 and R_s are the resistance values before and after the polarization, and ΔV (10 mV) is the constant applied voltage during polarization. The EIS was tested at the frequency of $0.1-10^6$ Hz with an amplitude of 5 mV at the OCP. The electrochemical floating test was conducted in Li||SS cell, which was charged to 4.1 V first, then held at progressively higher voltage, each for 10 h.

Theoretical Calculation:

MD simulations of two electrolyte systems were performed using Lammps with the all-atom optimized potentials for liquid simulations (pcff) force field. The charges of molecular were based on DFT calculation by Gaussian 09 suite of programs and Hirshfeld population analysis. Different electrolyte models were constructed with LiTFSI, G_4, the polymerized PETA segments and the copolymerization segments of AAPE and PETA. The initial simulation boxes of dimensions 80 × 80 × 80 $Å^3$ were constructed. Their structures were first relaxed by energy minimizing calculations, and then underwent an annealing from 0 to 298.15 K with the time step of 1 ps during 1 ns to reach the equilibrium state. Velocity-rescale thermostat with relaxation constant of 1 ps was used to control the temperature at 298.15 K. Berendsen's barostat with isothermal compressibility constant of 4.5×10^{-5} was used to control the pressure at 1.01325×10^5 Pa. Periodic boundary conditions were applied in all directions. Particle-mesh Ewald method with cut-off distance of 10 Å was applied to treat the electrostatic interactions and the van der Waals forces. Upon quasi-equilibrium of the system, MD simulation for a total simulation time of 50 ns was performed at constant NPT ensemble, and the trajectory was saved every 10 ps. The binding free energy of the complex was calculated from the formular:

$$E(\text{binding}) = E_{(A+B)} - E_{(A)} - E_{(B)}$$

where $E_{(A)}$ and $E_{(B)}$ is the energy of isolated molecules, $E_{(A+B)}$ is the total energy of the complex structure.

Table S1. The compositions of precursor solutions (with different ratios of crosslinker and matrix) and the corresponding ionic conductivities of the obtained electrolytes.

Sample	P(VDF-HFP) (wt%)	PETA (wt%)	AAPE (wt%)	SIL (wt%) [a]	Ionic conductivity (S/cm)
a	25	5	15	55	2.0×10^{-4}
b	20	5	15	60	5.0×10^{-4}
c	15	5	15	65	6.5×10^{-4}
d	12.5	5	15	67.5	8.0×10^{-4}
e	10	5	15	70	10×10^{-4} (crack)
f	20	10	15	55	2.0×10^{-4}
g	15	10	15	60	Crack
h	12.5	10	15	62.5	3.9×10^{-4}

[a] SIL: [Li(G4)] [TFSI]

Table S2. The compositions of precursor solutions (with different ratios of anion acceptor and solvate ionic liquid) and the corresponding ionic conductivities, electrochemical stability (ESW) window and lithium ion transference number (LITN) of the obtained electrolytes.

Sample	P(VDF-HFP) (wt%)	PETA (wt%)	AAPE (wt%)	SIL (wt%)	Ionic conductivity (S/cm)	ESW (V)	LITN
d-1	12.5	5	10	72.5	7.2×10^{-4} (crack)	-	-
d-2	12.5	5	12.5	70	9.2×10^{-4}	5.2	0.67
d-3*	12.5	5	15	67.5	8.0×10^{-4}	5.3	0.75
d-4	12.5	5	17.5	65	5.4×10^{-4}	5.4	0.80
d-5	12.5	5	20	62.5	4.3×10^{-4}	5.4	0.86

*sample d-3 was chosen as the electrolyte in the further cell testing

With the high content of anion acceptor, the content of solvate ionic liquid is reduced, resulting in low ionic conductivity which impairs the capacity and rate performance of battery. When the anion acceptor content is slightly decreased, the ionic conductivity

and Li^+ transference number can simultaneously maintain high values, improving Li^+ migration while confining the anions, which can ensure the excellent battery performance. However, a further reduction in anion acceptor content, despite maintaining high ionic conductivity, leads to insufficient anion immobilization. This allows anion concentration polarization to persist through the cycles, ultimately deteriorating the battery performance.

Figure S1. Optical image of large-size PBSIL membrane.

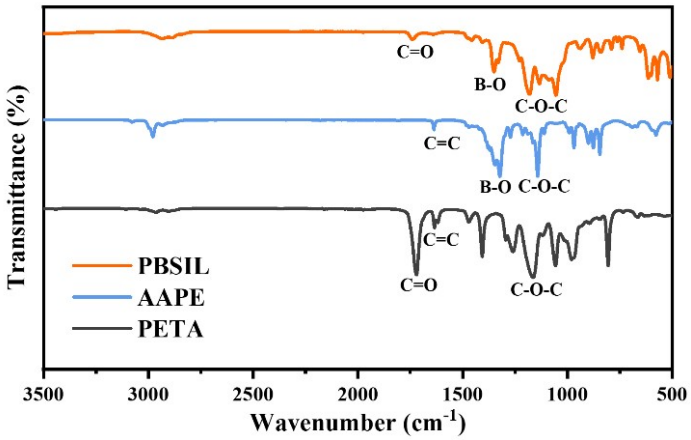

Figure S2. FTIR spectra of the PETA monomer, AAPE monomer and PBSIL.

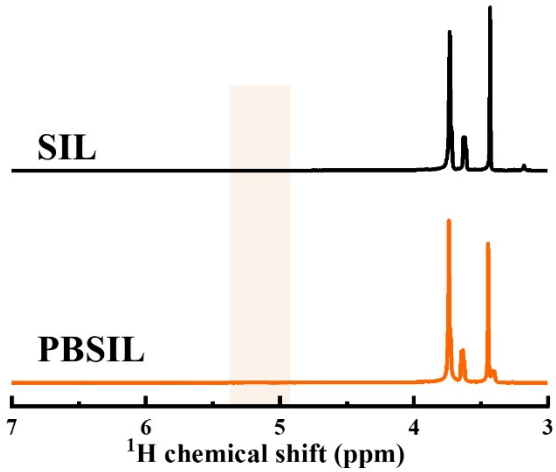

Figure S3. ^{1}H NMR spectra of SIL, and PBSIL. After the polymerization reaction, the chemical shifts of C=C bonds in PBSIL are barely detected, implying that almost all monomers are fixed on the crosslinked polymer network.

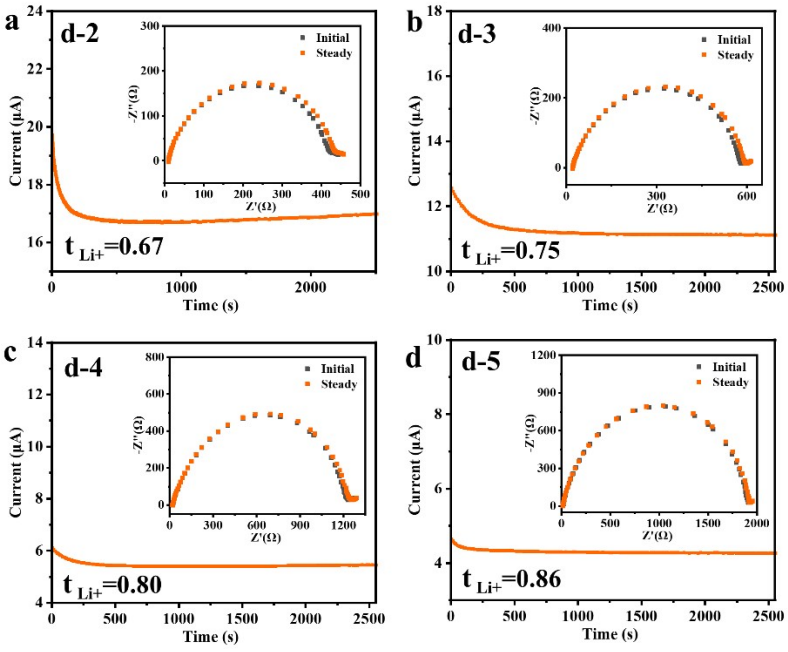

Figure S4. a-d) The lithium ion transference numbers of PBSIL with different ratios of anion acceptor.

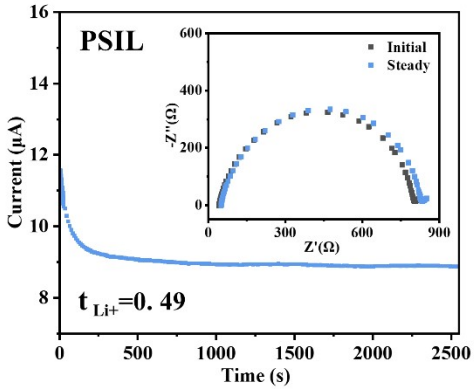

Figure S5. The lithium ion transference number of PSIL.

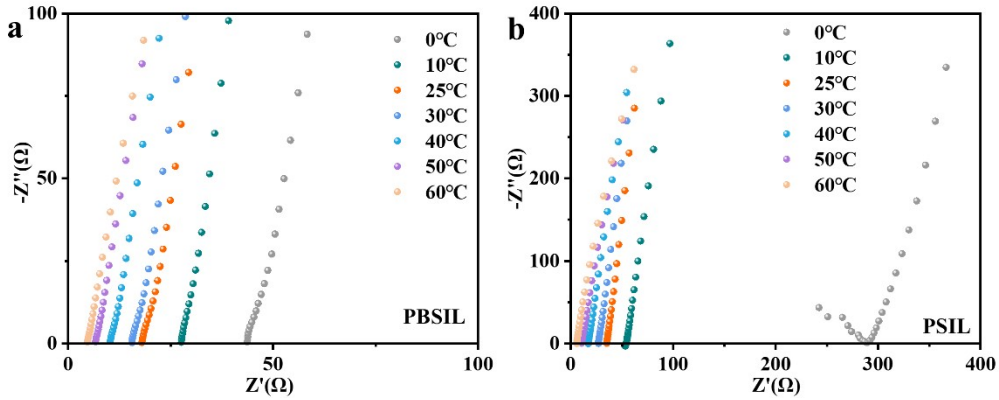

Figure S6. EIS spectra at different temperature of a) PBSIL, b) PSIL electrolytes.

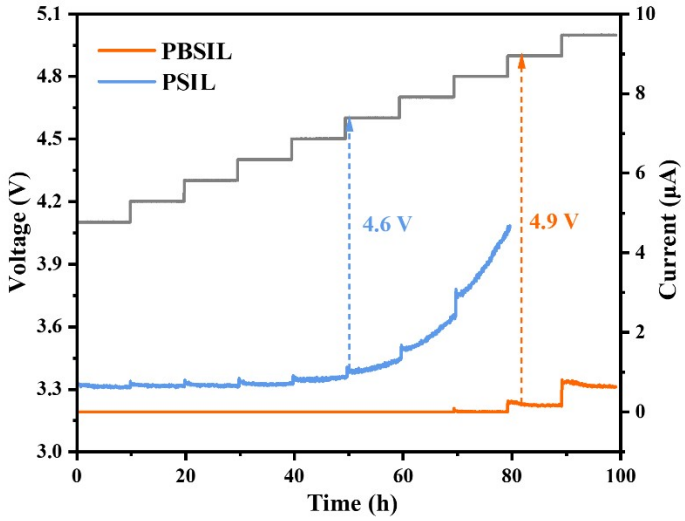

Figure S7. Electrochemical floating analyses of PBSIL and PSIL electrolyte.

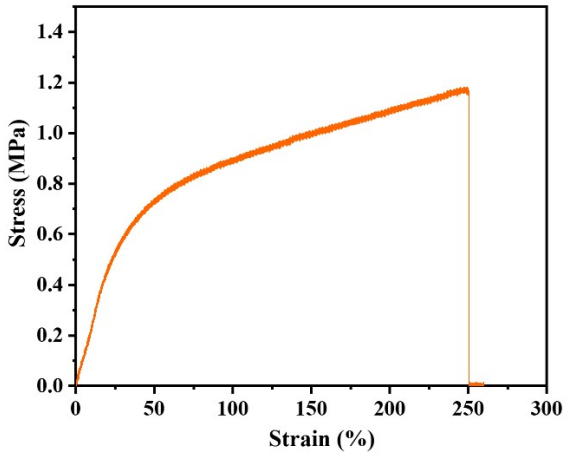

Figure S8. Stress-strain curve of PBSIL membrane.

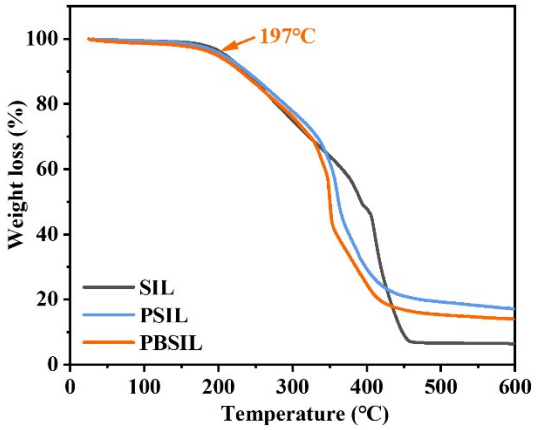

Figure S9. TGA profiles of SIL, PSIL and PBSIL.

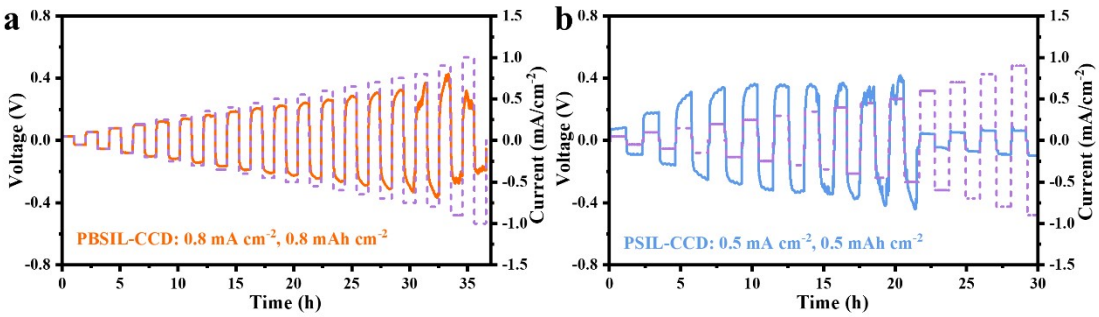

Figure S10. Critical current density tests of a) Li|PBSIL|Li, b) Li|PSIL|Li cell.

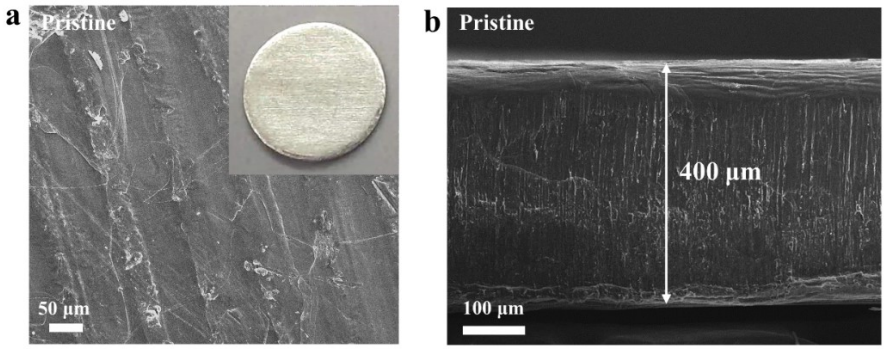

Figure S11. a) Top-view and b) cross-sectional SEM images of pristine Li. The inset is the optical image of pristine Li.

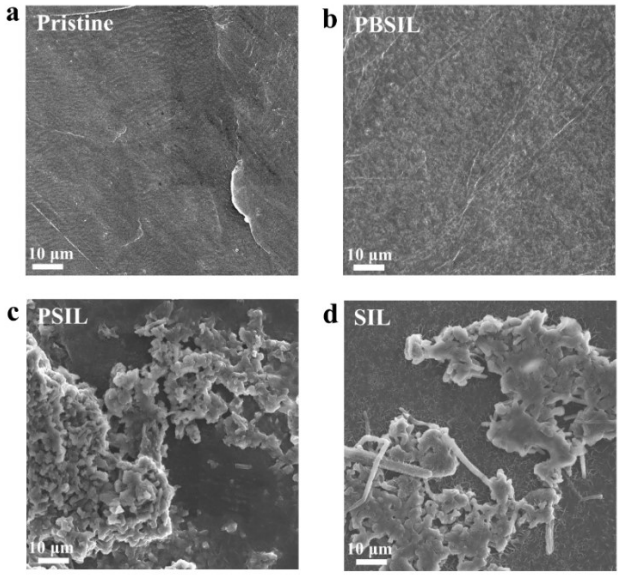

Figure S12. Top-view SEM images of a) pristine Li, Li metal electrodes after 50 cycles with b) PBSIL, c) PSIL, and d) SIL

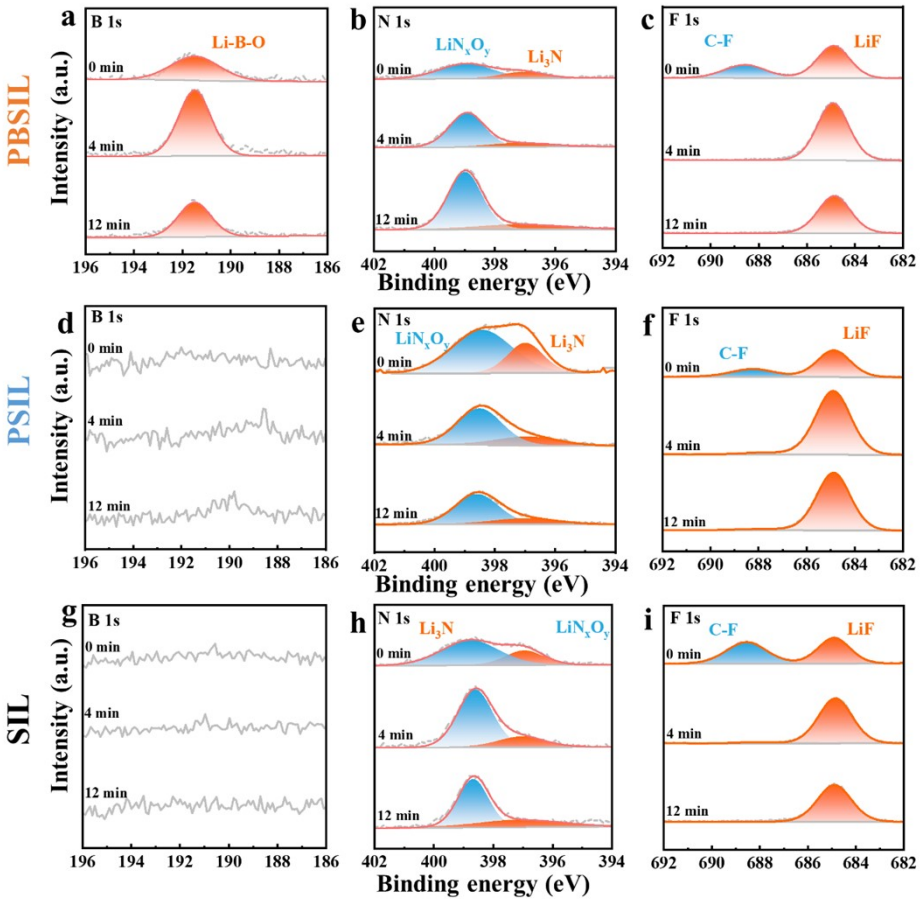

Figure S13. XPS depth profiles of the SEI on the cycled Li metal electrodes with a-c) PBSIL, d-f) PSIL, g-i) SIL.

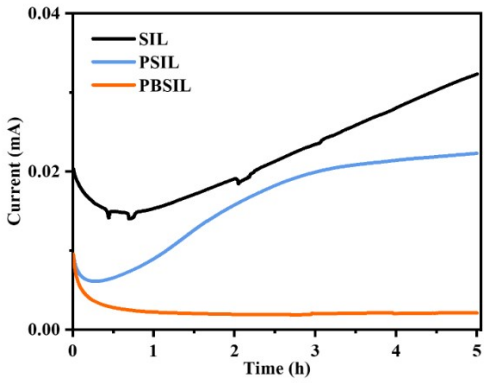

Figure S14. Chronoamperometry profiles of the Li||Al cells with different electrolytes at 5.0 V for 5 h.

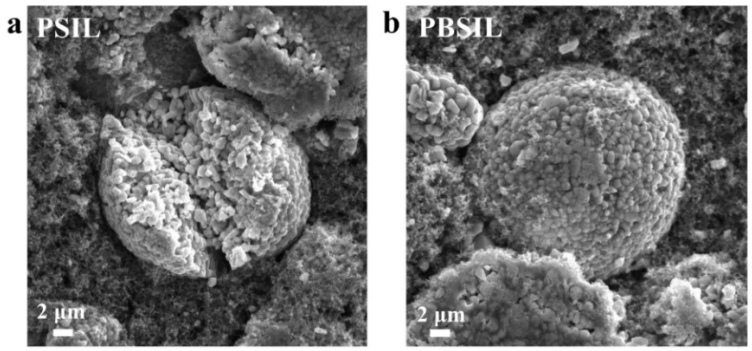

Figure S15. SEM images of the cycled NCM811cathodes with a, b) PSIL and c, d) PBSIL after 100 cycles.

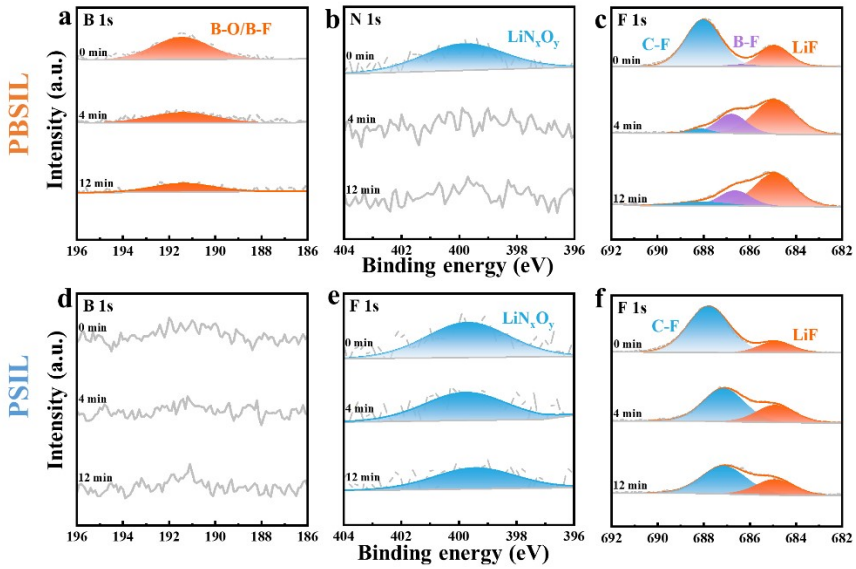

Figure S16. XPS depth profiles of the CEI on the cycled NCM811 electrodes with a-c) PBSIL, d-f) PSIL.

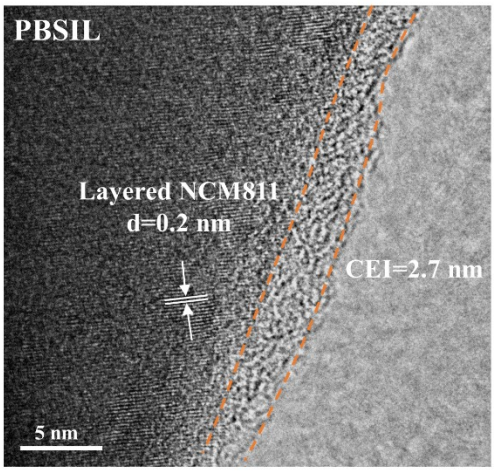

Figure S17. TEM image of the cycled NCM811cathode with PBSIL after 100 cycles.

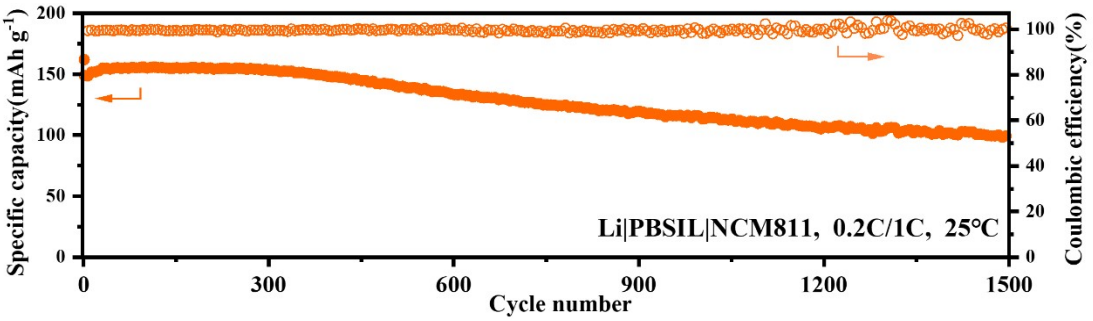

Figure S18. Long-cycling performance of Li|PBSIL|NCM811 cell with charging at 0.2 C and discharging at 1 C.

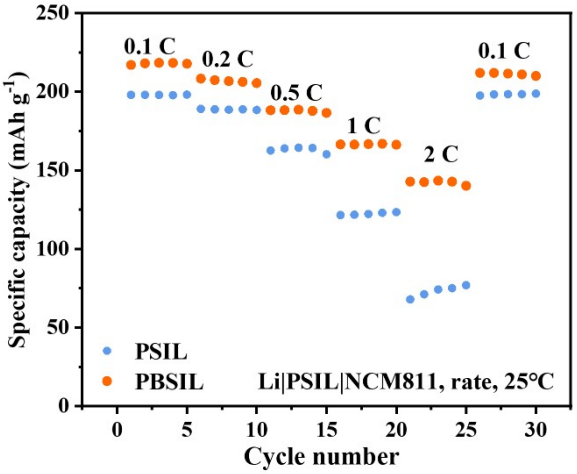

Figure S19. Rate performances of Li|PSIL|NCM811 cell and Li|PBSIL|NCM811 cell.

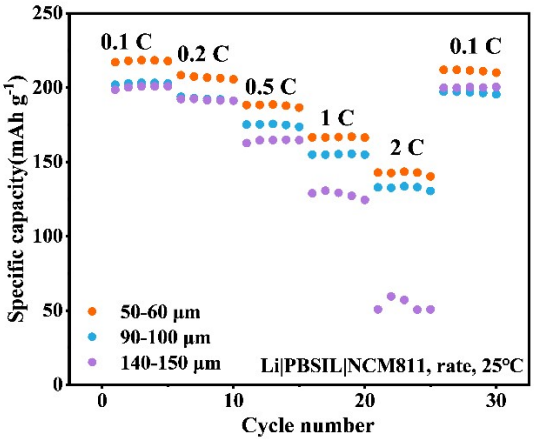

Figure S20. Rate performances of Li|PBSIL|NCM811 cells with different electrolyte thicknesses.

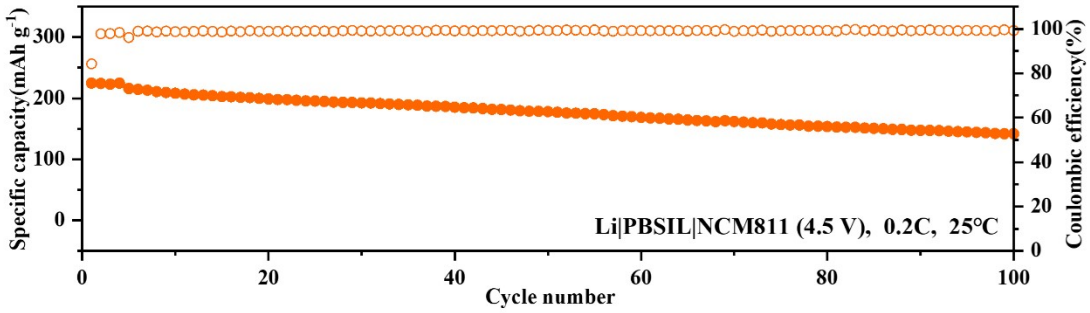

Figure S21. Cycling performance of Li|PBSIL|NCM811 cells with a charge cutoff voltage of 4.5 V.

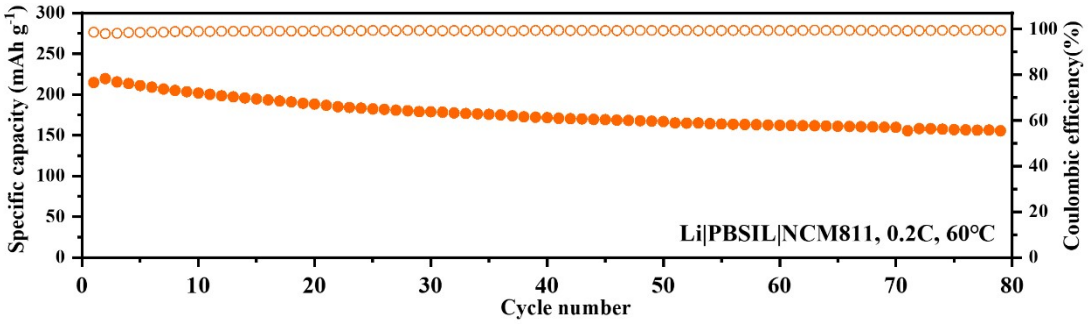

Figure S22. Cycling performance of Li|PBSIL|NCM811 cell at 60 °C.

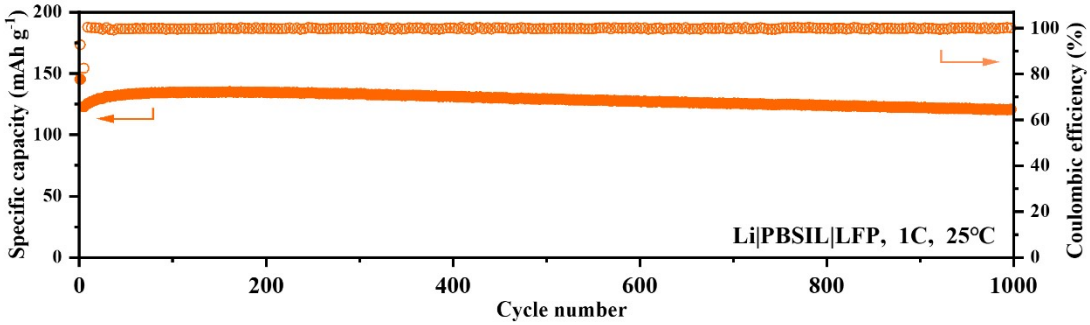

Figure S23. Long-cycling performance of Li|PBSIL|LFP cell at 1 C.

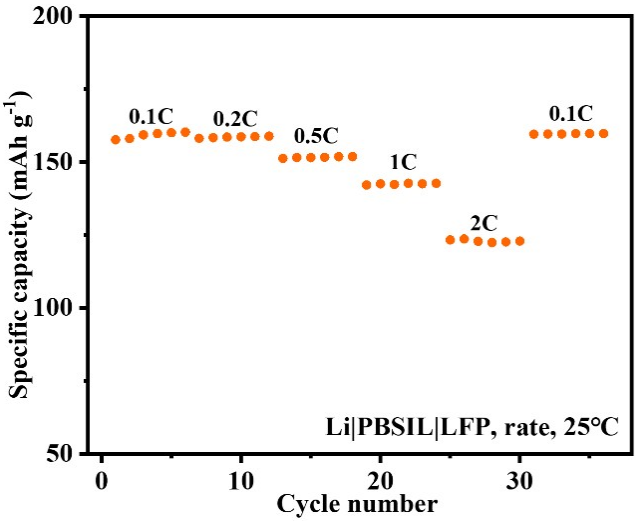

Figure S24. Rate performance of Li|PBSIL|LFP cell.

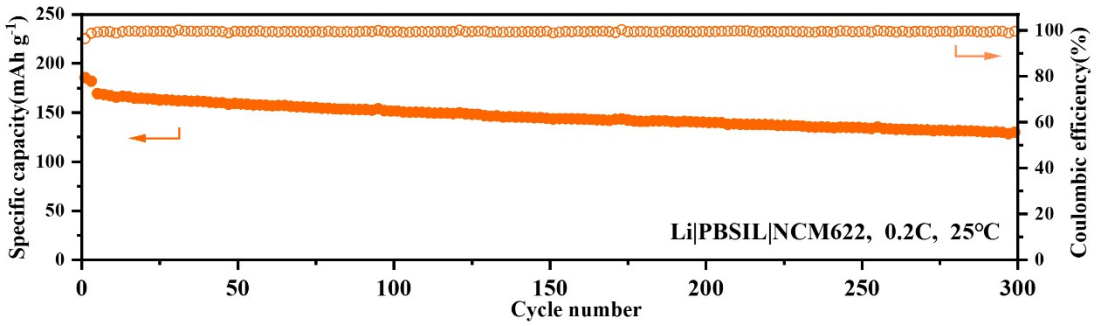

Figure S25. Cycling performance of Li|PBSIL|NCM622 cell at 0.2 C.

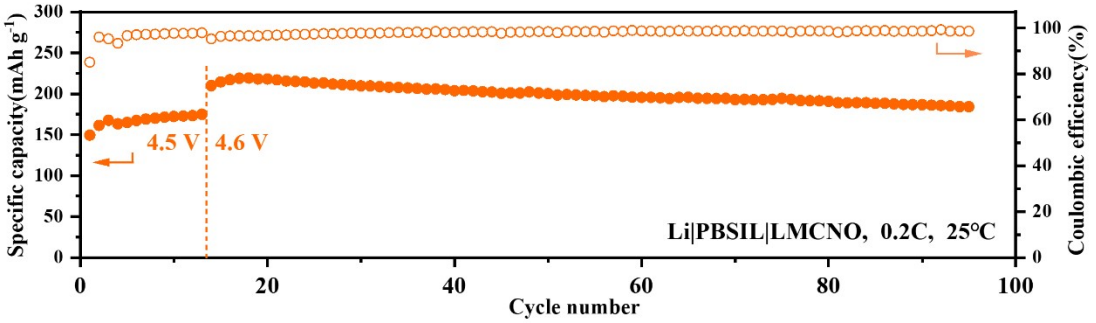

Figure S26. Cycling performance of Li|PBSIL|LMCNO cell at 0.2 C.

Table S3. Cylindrical cell parameters

Cell component	Specification	Parameters
Cathode	Cathode material	Single crystal NCM811
	Areal loading (each side, mg cm^{-2})	8
	Size (cm*cm)	5*12
Anode (Li)	Thickness (each side, μm)	20
	Size (cm*cm)	5.5*14
Electrolyte	Size (cm*cm)	6*16
Cell	N/P ratio	2.57
	Cutoff voltage (V)	4.3
	Areal capacity (mAh cm^{-2})	1.6

Table S4. Z-stacked pouch cell parameters

Cell component	Specification	Parameters
Cathode	Cathode material	Single crystal NCM811
	Areal loading (each side, mg cm^{-2})	8
	Size (cm*cm)	4*4
	number	3
Anode (Li)	Thickness (each side, μm)	20
	Size (cm*cm)	4.5*4.5
Electrolyte	Size (cm*cm)	5*16
Cell	N/P ratio	2.57
	Cutoff voltage (V)	4.3
	Areal capacity (mAh cm^{-2})	1.6

Table S5. The comparison of Li||NCM811 cells between this work and recently reported ex-situ solid polymer electrolytes in terms of conductivity, specific capacity, cycle number, and capacity retention.

Battery	Conductivity (mS cm^{-1})	Specific Capacity (mAh g^{-1})	Cycle number	Capacity retention (%)	Ref
Li|PBSIL|NCM811	0.8 at 25 ℃	209 at 0.2 C	100	94.4	This work
		183 at 0.2C/0.5 C	1300	75	
Li|LiPVAOB@PVDF /PE2|NCM811	1.14 at 25 ℃	208 at 0.5 C	1000	75	[1]
Li|6FPSF-FPES-70% EC|NCM811	0.69 at 40 ℃	173 at 0.2 C	160	83.6	[2]
Li| PALE-3-6|NCM811	0.84 at 25 ℃	154.1 at 1 C	500	42.8	[3]
Li|AMSE|NCM811	0.75 at 25 ℃	171 at 0.2 C	150	99	[4]
Li|PEGGPE@HT|NC M811	0.986 at 30 ℃	168.4 at 1 C	200	85.3	[5]
Li|MDPE|MDPE-NCM811	0.3 at 60 ℃	170 at 0.1 C	150	80	[6]
Li|PVDF-LPPO|NCM811	0.484 at 25 ℃	150 at 0.5 C	700	68	[7]
		137 at 1 C	1550	70.9	
Li|Poly(TEGDAPVA C)|NCM811	1.02 at 25 ℃	193 at 0.5 C	500	81.3	[8]
Li|sSIC-BPh_4|NCM811	4.4 at 25 ℃	178 at 1 C	250	88.6	[9]
Li|GTSSE|NCM811	0.0291 at 20 ℃	164.7 at 0.5 C	1000	65	[10]
Li|PHMP|NCM811	0.15 at 25 ℃	211.5 at 0.2 C	250	81	[11]
Li|C5-POE-F-Li|NCM811	0.036 at 45 ℃	190.5 at 0.16 C	100	82.8	[12]
Li|UFF/PEO/PAN/Li TFSI| NCM811	0.068 at 25 ℃	109 at 1 C	300	84.4	[13]
Li|UFF/PEO/MOFs-NH2| NCM523	0.065 at 25 ℃	172 at 0.2 C	100	80.3	[14]
Li|C5-POE-F-Li |NCM622	0.035 at 45 ℃	166 at 0.1 C	200	70.2	[15]
Li|F&NPE |NCM622	1.01 at 25 ℃	170 at 0.5 C	700	83.9	[16]

[1] M. Cui, N. Gao, W. Zhao, H. Zhao, Z. Cao, Y. Qin, G. Gao, K. Xi, Y. Su, S. Ding, *Adv. Energy Mater.* **2024**, 2303834.

[2] X. Dong, A. Mayer, X. Liu, S. Passerini, D. Bresser, *ACS Energy Lett.* **2023**, *8*, 1114-1121.

[3] S. M. Chai, Z. Chang, Y. Zhong, Q. He, Y. J. Wang, Y. L. Wan, M. Y. Feng, Y. Z. Hu, W. H. Li, W. F. Wei, A. Q. Pan, *Adv. Funct. Mater.* **2023**, *33*, 2300425.

[4] M. Yao, Q. Q. Ruan, S. S. Pan, H. T. Zhang, S. J. Zhang, *Adv. Energy Mater.* **2023**, *13*, 2203640.

[5] T. Zhu, G. Q. Liu, D. L. Chen, J. X. Chen, P. Qi, J. Sun, S. Zhang, *Energy Storage Mater.* **2022**, *50*, 495-504.

[6] C. Wang, H. Liu, Y. Liang, D. Li, X. Zhao, J. Chen, W. Huang, L. Gao, L. Z. Fan, *Adv. Funct. Mater.* **2022**, *33*, 2209828.

[7] J. S. Mi, J. B. Ma, L. K. Chen, C. Lai, K. Yang, J. Biao, H. Y. Xia, X. Song, W. Lv, G. M. Zhong, Y. B. He, *Energy Storage Mater.* **2022**, *48*, 375-383.

[8] Z. Li, S. T. Weng, J. L. Fua, X. X. Wang, X. Y. Zhou, Q. H. Zhang, X. F. Wang, L. Wei, X. Guo, *Energy Storage Mater.* **2022**, *47*, 542-550.

[9] S. K. Cho, K. S. Oh, J. C. Shin, J. E. Lee, K. M. Lee, J. Cho, W. B. Lee, S. K. Kwak, M. Lee, S. Y. Lee, *Adv. Funct. Mater.* **2022**, *32*, 2107753.

[10] F. Liu, Y. Cheng, X. Zuo, R. Chen, J. Zhang, L. Mai, L. Xu, *Chem. Eng. J.* **2022**, *441*, 136077.

[11] K. Zhang, F. Wu, X. Wang, L. Zheng, X. Yang, H. Zhao, Y. Sun, W. Zhao, Y. Bai, C. Wu, *Adv. Funct. Mater.* **2021**, *32*, 2107764.

[12] H. Sun, X. Xie, Q. Huang, Z. Wang, K. Chen, X. Li, J. Gao, Y. Li, H. Li, J. Qiu, W. Zhou, *Angew. Chem. Int. Ed.* **2021**, *60*, 18335-18343.

[13] F. He, W. Tang, X. Zhang, L. Deng, J. Luo, *Adv. Mater.* **2021**, *33*, e2105329.

[14] L. Xu, X. Xiao, H. Tu, F. Zhu, J. Wang, H. Liu, W. Huang, W. Deng, H. Hou, T. Liu, X. Ji, K. Amine, G. Zou, *Adv. Mater.* **2023**, e2303193.

[15] X. Xie, Z. Wang, S. He, K. Chen, Q. Huang, P. Zhang, S. M. Hao, J. Wang, W. Zhou, *Angew. Chem. Int. Ed. Engl.* **2023**, *62*, e202218229.

[16] S. Qi, M. Li, Y. Gao, W. Zhang, S. Liu, J. Zhao, L. Du, *Adv. Mater.* **2023**, e2304951.